ACCURACY OF MEASUREMENT IN INSTRUMENTED IMPACT TEST

T. Kobayashi and S. Morita

Department of Production Systems Engineering, Toyohashi University of Technology,
Toyohashi, 441-8580, Japan

ABSTRACT

The load calibration and instrumented Charpy impact tests were performed to investigate the measurement method of the accurate impact load. Decrease in specimen thickness results in slight decrease of calibration factors. This was attributed to strain localization within a near the region in which strain gages were attached. The results strongly suggested that the system must be calibrated for the different thickness of specimens to know accurate impact load. The accurate impact load was not measured around the end of slit which was introduced to release the constraining effect of deformation of the gage position from surrounding hammer; the effect of the vibration of the hammer appeared strongly around this position. However, it was possible to prevent the effect of such vibration by attaching the gage away from such position.

KEYWORDS

instrumented Charpy impact test, load calibration, instrumented striker, strain gage position, FEM.

INTRODUCTON

One of the authors has already developed the CAI (Computer Aided Instrumented Impact Testing) System, where dynamic fracture toughness parameters are obtained simply from the analysis of the load-deflection curve of a single precracked specimen [1]. In the test, therefore, it is important to record an accurate impact load. Generally one can obtain the measured load by multiplying the strain signal from attached strain gages on the instrumented striker by a load calibration factor assuming a linear relationship between the strain gage signal and applied load.

Recently, the instrumented Charpy impact test is used for the evaluation of toughness of many kinds of materials and miniaturized specimens. In those cases, a significant variation in the calibration factor has been reported because the Charpy specimen was changed from the standard steel specimen to another material or geometry [2-4]. Though a lot of methods of load calibration are proposed [5, 6], there is no report taking into consideration the change of material or geometry of the specimen. The elucidation of the mechanism that the load calibration factor changes by material or geometry of the specimen is important to measure accurate impact load and to enact the standard of load calibration method.

Although JIS or ISO describes about the instrumented striker, amplifier, data processing parameter and etc., detailed method on load measurement is hardly described in any standard. In the current standard of ASTM and ISO, there is no regulation on the accurate strain gage position for instrumentation (sometimes 11-15

mm from the tip is recommended).

In the present study, the load calibration test was performed when the material and geometry of the specimen was changed from the standard steel specimen. Then, the strain distributions in the instrumented striker were simulated by finite element analysis to explain the mechanism of the change in a load calibration factor. Moreover, instrumented Charpy impact test was carried out using the strikers which the strain gages were attached to four positions in order to investigate the effect of gage position on actual impact load. The changes in strain with respect to the time were simulated by finite element analysis to explain the effect of the vibration of hammer on the measured load for the specified strain gage positions.

EXPERIMENTAL AND ANALYTICAL PROCEDURES

Load Calibration Test

An instrumented Charpy impact test machine with 98 J capacity was used for the load calibration. The semi-conductor strain gages were attached on both sides and 16 mm from the tip of instrumented striker. The instrumented striker was loaded with the compressive load P through the specimen under the static condition. From the linear relationship between P and the output voltage V from the bridge circuit, the load calibration factor C can be calculated as

$$C = \Delta P / \Delta V \quad (1).$$

In this calibration, 6 kN and 3 kN of maximum compressive load were applied in the case of the specimen thickness 10 to 3 mm and 1.5 mm, respectively.

Instrumented Charpy impact test

An instrumented Charpy impact test machine with 100 J capacity was used for the instrumented Charpy impact test. Instrumented Charpy impact test was carried out using two types of strikers shown in Fig. 1. The hollowed striker is the conventional type. On the other hand, Non- hollowed striker was designed to prevent the strain localization [2]. The semi-conductor strain gages were attached on both sides and the positions from the tip of instrumented striker were 15, 30 and 45 mm, respectively. The loading velocity was 4.5 m/s.

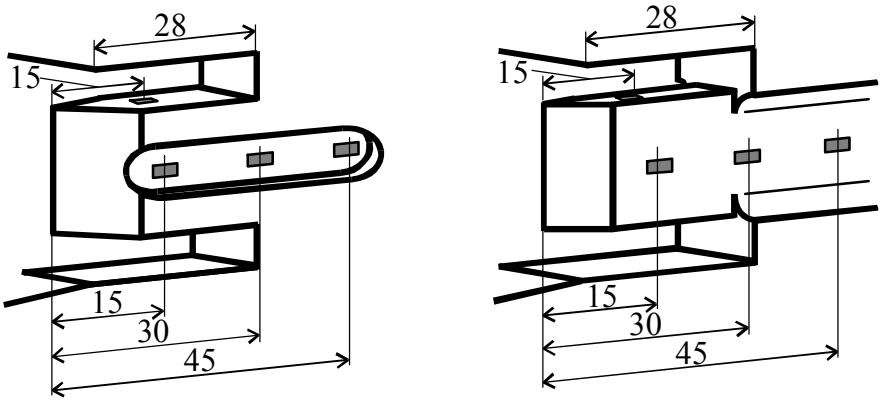

Hollowed striker **Non-hollowed striker**

Figure 1: Schematic illustration of instrumented striker for instrumented Charpy impact test (mm).

Finite Element Analysis

To calculate strain fields in the instrumented striker, the ANSYS non-linear finite element code was used for the analysis. A whole finite element model of the instrumented Charpy hammer and the specimen are shown in Fig. 2. The hammer arm was disregarded in the model. The model was three-dimensional 1/4 size using the symmetric condition. Eight-noded brick elements were used in modeling the hammer and the specimen. The contact elements were formed at contact points between a surface of the instrumented striker and the specimen to calculate contact forces. Full-Newton-Raphson method was used for the convergence calculation. The elastic modulus of the instrumented striker was taken to be 210 GPa. The

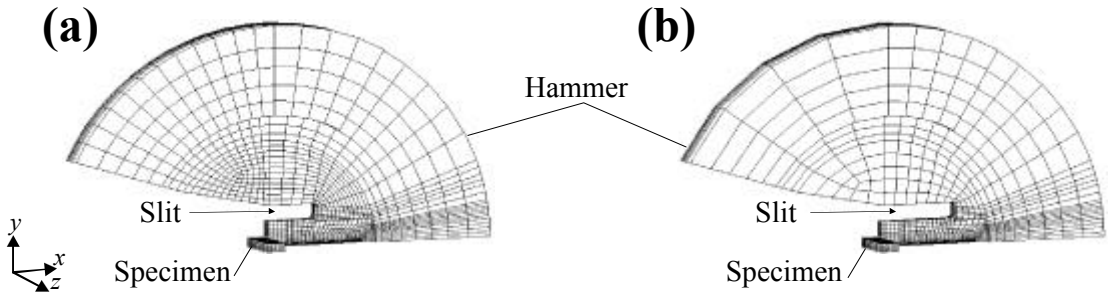

Figure 2: (a) Finite element model of Charpy hammer with specimen for low blow instrumented Charpy test. (b) Finite element model by introducing deep cutting slit.

elastic modulus of the specimen used were 210 (A508 steel) and 70 GPa (6061 Al).

RESULTS AND DISCUSSION

Effects of Materials and Sizes of the Specimen on Load Calibration Factor

Figure 3 shows the relationship between the load calibration factor *C* and thickness of the specimen *B* in the case of a specimen made of A508 steel and 6061 aluminum alloy. It is clear from Fig. 3 that *C* linearly decreases with thickness of the specimen in both materials. These results suggest that a change of strain field around the strain gage position occurs complex contact mechanism of the instrumented striker with the specimen.

Many types of specimens of different materials and sizes from the standard specimen are used to evaluate the dynamic properties such as the aging degradation of the structural materials and neutron radiation embrittlement of the nuclear reactor in the instrumented Charpy impact test. In those tests, measured impact load is calculated on the assumption that *C* does not change by the materials or sizes of the specimen. However, Fig. 3 shows that materials and sizes of the specimens affect a load calibration factor, therefore, it is recommended that the instrumented striker must be calibrated for the different materials and sizes of specimens to obtain accurate impact load data.

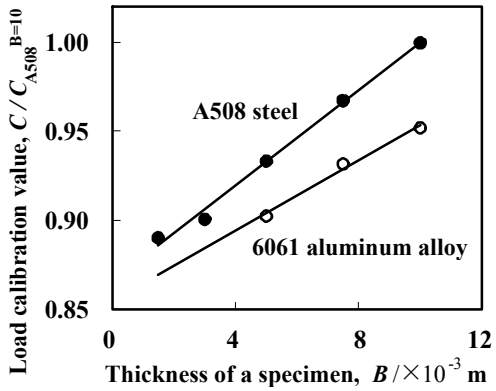

Figure 3: Effects of the thickness of specimens, B, on the load calibration factor, C, of A508 and 6061 Al. C is normalized with a load calibration factor of a specimen thickness of 10 mm and made of A508 steel, $C_{A508}^{B=10}$.

Effects of Specimen Sizes on Strain Distribution in the Instrumented Striker

Figure 4 shows contour maps of predicted strain in *x* direction ε_x within the instrumented striker. In those figures, a part of the hammer except for the instrumented striker is not shown. A strain distribution changes complicatedly due to the decrease of the thickness of specimen. The strain is localized in the center of the instrumented striker with the decrease from *B*=10 mm to *B*=3 mm. It can be seen that the strain is concentrated at the corresponding region to the thickness of the specimen. The maximum compressive strain ε^m_x in the case of (b) reaches 2.7 times in comparison with ε^m_x in the case of (a). In the upper part of the instrumented striker, the tensile strain is developed with the decrease of the specimen thickness.

The situation of the instrumented striker differs from the standard load cell, in which the output is the same no matter how specimen material and geometry are changed. The experimental and analytical results

indicate that the material and the geometry of the specimen influence the strain fields in the instrumented striker, and change of the load calibration factor. When this phenomenon is disregarded, the measured load consequentially produces the error. Of course, sensitivity of the instrumented striker depends not only on the change of specimen materials and sizes, but also on the design of the instrumented striker.

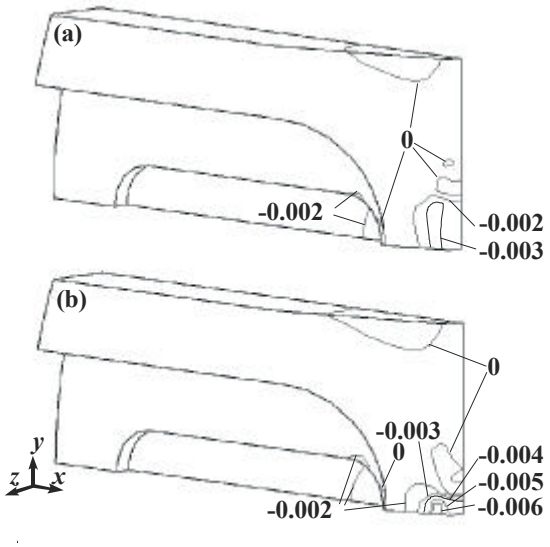

Figure 4: Contour maps of the strain in x direction ε_x, within the instrumented striker. Specimen thickness, B, is (a) 10 mm and (b) 3 mm. Applied load, P, is 6 kN.

Effect of the Strain Gage Position on the Measured Impact Load

Figure 5 shows the typical load-deflection curves recorded from two types of instrumented strikers for 6061-T6 aluminum alloy. The load-deflection curve recorded from gage position 15 mm is smooth. On the other hand, it is obvious that the vibration was superimposed on the load-deflection curves recorded from the other strain gage positions after the maximum load. There are no differences between two types of striker geometries. The absorbed energies were estimated from load-deflection curves of all strain gage positions. The absorbed energy estimated from load-deflection curve of gage position 15 mm is approximately same as the dial energy. The strain gage position 15 mm recorded the accurate impact load history.

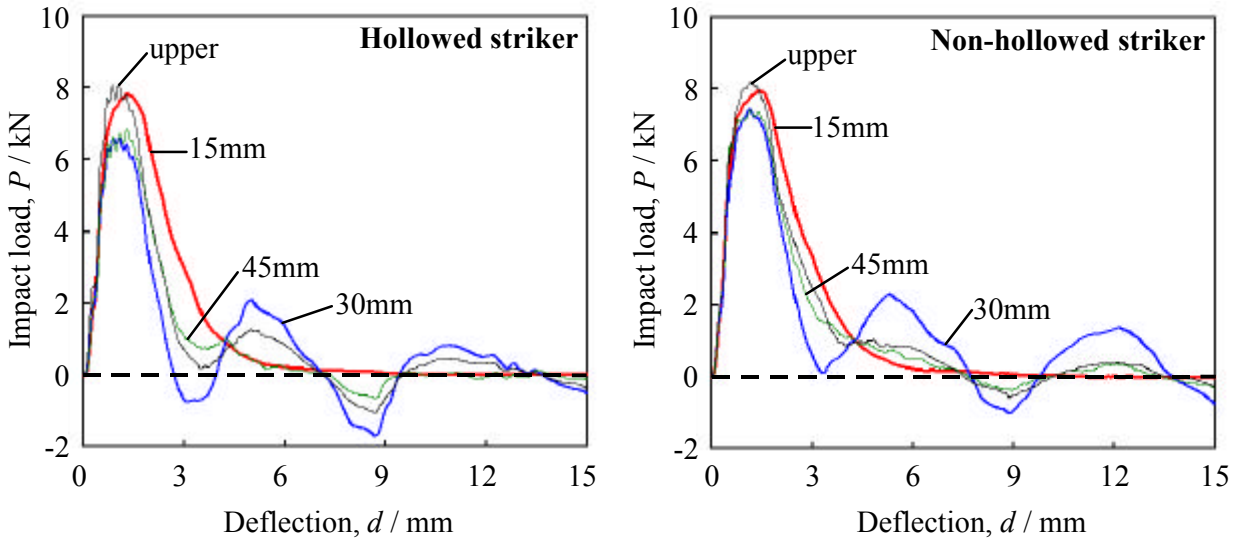

Figure 5: Typical load-deflection curves recorded from specified strain gage positions in hollowed and non-hollowed strikers for the V-notched 6061-T6 Al alloy Charpy specimen.

Figure 6 shows the prediction of the change in compressive strain along (x) and orthogonal to (y, z) direction of blow calculated by finite element analysis for specified strain gage positions. It can be seen that the strain of the x direction is symmetry for the time shown in Fig.6(a). In Fig.6(b), the vibrations were

observed in the strain of the *y* direction recorded from gage positions 30 and 45 mm. These were affected by vibration of the hammer as shown in Fig.7. The respect to time of the vibration of displacement is the same manner of gage positions 30 and 45 mm as shown in Fig.6(b). The previous work [7] reported that the hammer deforms elastically and then vibrates periodically. It is concluded that the both ends of the hammer are deformed conversely and the hammer edge portion (near the end of the slit), where the strain gage is attached, is bent by the natural vibration of the hammer. Consequently, it is recommended that the strain gage is attached near the tip of striker.

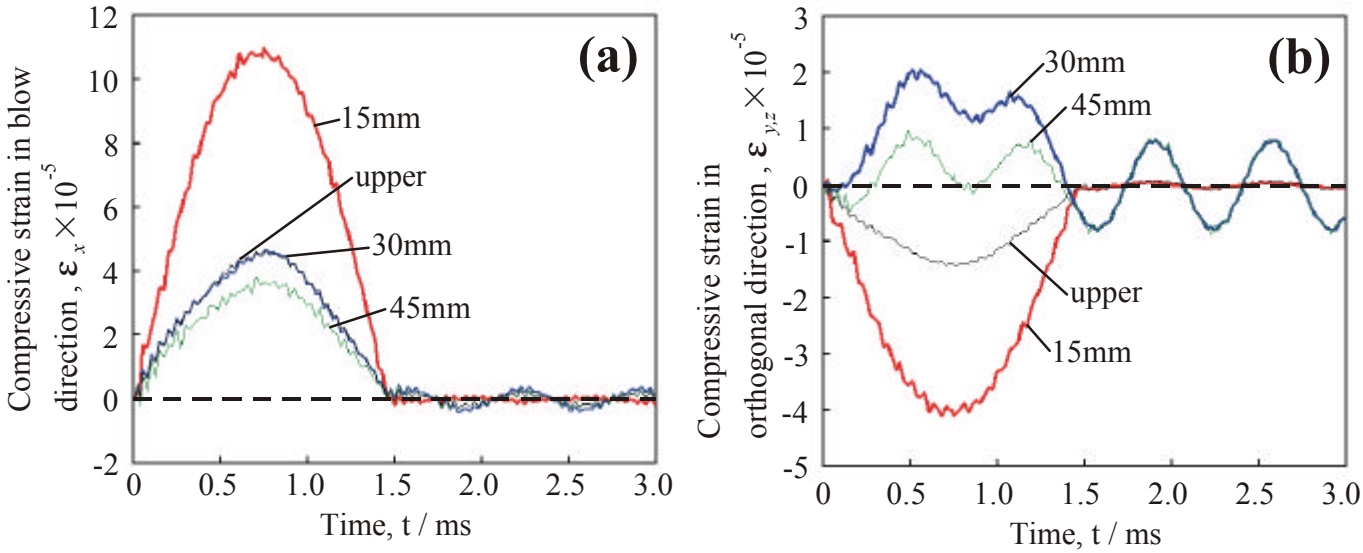

Figure 6: Changes in compressive strain with respect to time for specified strain gage positions in FEM analysis. (a)Compressive strains along the direction of blow (*x*-direction). (b)Compressive strains, orthogonal to the direction of blow for 15, 30, 45mm and upper positions, respectively, in *y* and *z*-directions.

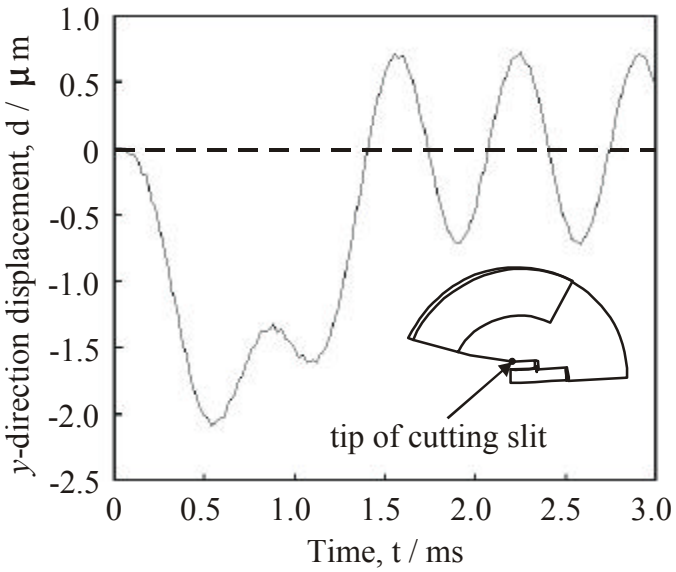

Figure 7: Variation of *y*-direction displacement at the tip of cutting slit with respect to time upon impact.

Effect of the Slit Depth of striker on the Measured Impact Load

Figure 8 shows the prediction of the change in compressive strain calculated by model of Fig.2(b). The depth of slit is deeper than Fig.2(a). The constraining of deformation of the gage position 30 mm from surrounding hammer was released by the slit. In Fig.8(a), the strain of the *x* direction is symmetry for the time as shown in Fig.6(a). In the strain of the *y* direction, the vibration was still observed in the strain-time curve obtained from gage position 45 mm. The accurate impact load was not measured around the end of slit which was introduced to release the constraining effect of deformation of the gage position from surrounding hammer; the effect of the vibration of the hammer appeared strongly around this position. However, it was possible to prevent the effect of such vibration by attaching the gage away from such position.

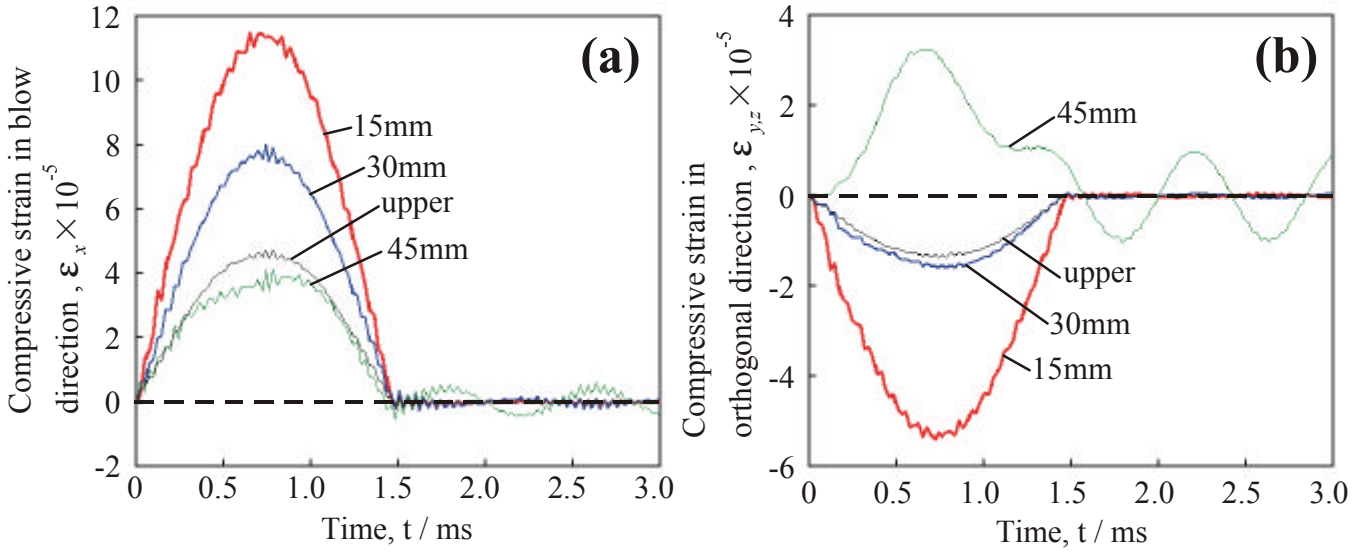

Figure 8: Changes in compressive strain with respect to time for specified strain gage positions in FEM analysis. (a) Compressive strains along the direction of blow (*x*-direction). (b) Compressive strains, orthogonal to the direction of blow for 15, 30, 45mm and upper positions, respectively, in *y* and *z*-directions.

CONCLUSIONS

(1) In the calibration tests, the load calibration factor linearly decreases with the thickness of specimen. These results mean that the measured load gives an overestimate for the total absorbed energy and impact load when the material and the size effects on a load calibration factor are disregarded.

(2) Finite element analysis indicates that even if the applied load is the same, a compressive strain is localized in the center of the instrumented striker with the decrease of specimen thickness. Therefore, the load calibration factor decreases.

(3) The materials and the sizes of specimens influence the strain fields in the instrumented striker, and make change in the load calibration factor. A compressive strain in the instrumented striker changes largely near the contact point with the specimen. These results strongly suggest that the system must be calibrated for the different materials and sizes of specimens to obtain accurate impact load.

(4) The accurate impact load was not measured around the end of slit which was introduced to release the constraining effect of deformation of the gage position from surrounding hammer; the effect of the vibration of the hammer appeared strongly around this position.

REFERENCES

1. Kobayashi, T., Yamamoto, I. and Niinomi, M. (1993) *J. Test. Eval.* 21, 145.
2. Kobayashi, T., Morita, S., Inoue, N. and Toda, H. (2000). In: *Pendulum Impact Testing: A Century of Progress, STP 1380*, pp.198-209, Siewert, T. A. and Manahan, M. P. Sr. (Eds). ASTM, West Conshohocken, PA.
3. Marur, P. R., Shimha, K. R. Y. and Nari, P. S. (1995) *J. Test. Eval.* 23, 267.
4. Kalthoff, J. F., Walle, E. van and Wilde, G. (1996). In: *Evaluating Material Properties by Dynamic Testing*, *ESIS20*, pp.25-35, Walle, E. van (Ed). Mechanical Engineering Publications, London.
5. Winkler, S. and Bo β, B. (1996). In: *Evaluating Material Properties by Dynamic Testing*, *ESIS20*, pp.37-44. Walle, E. van (Ed). Mechanical Engineering Publications, London.
6. Wilde, G., Covic, M. and Gregor, M. (1996). In: *Evaluating Material Properties by Dynamic Testing*, *ESIS20*, pp.89-96, Walle, E. van (Ed). Mechanical Engineering Publications, London.
7. Yamamoto, I. and Kobayashi, T. (1993) *Int. J. Pressure Vessels Piping*, 55, 295.